Journal of the Korean Chemical Society
2002, *Vol. 46, No. 3*
Printed in the Republic of Korea

PT, PZ와 PZT나노튜브의 졸-겔 형판합성과 특성

張起錫* · Bernadette A. Hernandez‡ · Ellen R. Fisher† · Peter K. Dorhout‡
공군사관학교 화학과
‡미국 콜로라도주립대 화학과
(2002. 4. 15 접수)

Sol-Gel Template Synthesis and Characterization of PT, PZ and PZT Nanotubes

Ki-Seog Chang*, Bernadette A. Hernandez†, Ellen R. Fisher‡, and Peter K. Dorhout†
Department of Chemistry, Korea Air Force Academy
‡Department of Chemistry, Colorado State University, USA
(Received April 15, 2002)

요 약. 졸-겔 형판 합성법을 이용하여 페로브스카이트 구조를 갖는 나노튜브를 합성하고 그 특성을 조사하였다. $PbTiO_3$(PT), $PbZrO_3$(PZ)와 $PbZrO_3$-$PbTiO_3$(PZT) 고용체 나노튜브는 반응물, $Ti(OPr^i)_4$, $Zr(OBu)_4$와 $Pb(OAc)_2$-$3H_2O$ 들의 킬레이트 졸-겔 합성법에 의해서 합성하였다. 산화 알루미늄 형판은 200 nm의 직경을 갖는 휘트만® 아노디스크가 사용되었다. 6.0 M-NaOH 용액에서 형판을 제거한 다음, 주사현미경 분석에 의해서 50 m 길이와 200 nm 외곽 직경의 생성물 나노튜브를 확인할 수 있었다. 투과현미경 분석과 전자회절 분석에 의하여 나노튜브가 다결정임을 확인하였다. DSC 분석에 의해서 PT 나노튜브의 상전이 온도는 특이하게도 234.4 °C 임이 확인되었으며, 이때의 입자크기는 X-선 분석의 하나인 Scherrer 식에 의해서 15.4 nm 임이 계산되었다.

주제어: 티탄산, 나노튜브, 형판, 강유전체

ABSTRACT. We report the synthesis and characterization of the perovskite nanotubes made by sol-gel template synthesis. Both lead titanate ($PbTiO_3$; PT), lead zirconate ($PbZrO_3$; PZ) and lead zirconium titanate ($PbZrO_3$-$PbTiO_3$; PZT) solid solution nanotubes were prepared with a chelate sol-gel of titanium isopropoxide ($Ti(OPr^i)_4$), zirconium tetrabutoxide ($Zr(OBu)_4$) and the respective lead acetate ($Pb(OAc)_2$-$3H_2O$). Whatman® anodise membranes, with a 200 nm pore size, served as the template. After the removal of the template in the 6M-NaOH, scanning electron microscopy shows that the shapes formed are 200 nm outer diameter tubes with 50 μm lengths. Transmission electron microscopy and electron diffraction reveal that the tubes are polycrystalline. The PT nanotubes so far have shown an anomalous transition temperature, 234.4 °C as measured by DSC with a small particle size, 15.4 nm determined by X-ray analysis with the aid of Scherrer's equation.

Keywords: Titanate, Nanotubes, Template, Ferroelectrics

INTRODUCTION

A series of sol-gel routes to oxide-based pyroelectrics and ferroelectrics belong to the structural family known as the perovskite structures. They have the general formula ABO_3, which has generally shown in both its cubic or tetragonal phases. In both structures, AE^{2+} (AE: Ca, Sr and Ba) and Pb^{2+} cations occupy the A site on each corner of the unit cell. The Zr^{4+} or Ti^{4+} ion occupies in the center of an octahedron and a distorted octahedron

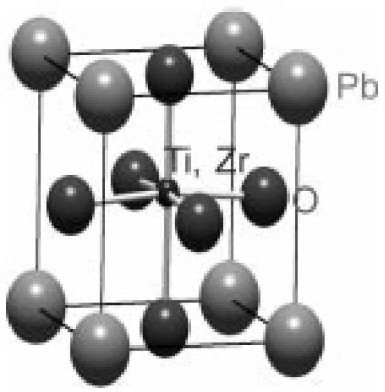

Fig. 1. Configuration of the ABO_3 perovskite unit cell for the $PbZr_{1-x}Ti_xO_3$ system. Ionic radii (Å): Pb^{2+} (1.49), Ti^{4+} (0.61), Zr^{4+} (0.72), O^{2-} (1.42).

formed by the six O^{2-} anions in the B site. Both cubic (paraelectric phase) and tetragonal (ferroelectric phase) forms are known to have high dielectric constants at room temperature. However, it is the tetragonal form that possesses a ferroelectrics behavior (*Fig.* 1).

Advances toward nano-scale electronics have caused interest in size effects on the properties of ferroelectric ceramics. These materials are employed for their dielectric, piezoelectric, electrorestrictive, pyroelectric, and electrooptic properties with applications accounting for 60% of the total high technology functional ceramics market globally.[1,2] The properties of ferroelectric ceramics arise from having non-centrosymmetric unit cells that produce a polarization state.[3] Understanding how the crystal structure and state of polarization is influenced by particle size is vital to the performance of the ferroelectric ceramics.

EXPERIMENTS

Materials Used. Ethyl alcohol (EtOH) (dehydrated) and 2-methoxyethanol ($CH_3OCH_2CH_2OH$) were purchased from Pharmco. Glacial acetic acid (HOAc) and sodium hydroxide (NaOH) pellets from Mallinckrodt were used as received. Titanium (IV) isopropoxide, $(Ti(OPr^i)_4)$ was purchased from Aldrich and distilled prior to use. Titanium (IV) butoxide, $(Ti(OBu)_4)$ and Zirconium (IV) butoxide, $(Zr(OBu)_4)$ were purchased from Aldrich. Lead acetate, $Pb(OAc)_2$-$3H_2O$, and Whatman® (0.2 μm pore size, 50 μm length, 25 mm diameter) anodisc membranes were purchased from Fisher and used as received. Purified water was obtained by passing house-distilled water through a Milli-Q (Millipore) water purification system. 1500 grit sandpaper (3 M) was purchased from Auto-Zone. Quick-dry epoxy from Cole-Parmer Instrument Co. was used. Formvar coated 200 mesh copper grids and double-sided copper tape was purchased from Ted Pella Inc.

Solid Solution. Powders and tubes in the solid-solution series $PbTiO_3$-$PbZrO_3$ system were prepared by heating a stoichiometric mixture of the reagents $Pb(OAc)_2$-$3H_2O$, $Zr(OBu)_4$, and $Ti(OBu)_4$ or $(Ti(OPr^i)_4)$, respectively. The dip-coating tubes and the mixtures were heated in alumina crucibles at suitable temperatures and then cooled. X-ray powder diffraction patterns and X-ray thin film diffraction patterns of the products were collected with a Phillips diffractometer. Also, they were characterized by using a Raman spectrometer.

Synthesis. $PbZrO_3$, $PbTiO_3$, and solid solution system tubes were prepared using a sol-gel method similar to that described by Sharma *et al.*[4] For example, a lead solution was prepared by dissolving 6.069 g of $Pb(OAc)_2$-$3H_2O$ in 13 mL of HOAc (~40 °C) or 13 mL of $CH_3OCH_2CH_2OH$ (~124 °C) for a 0.8 M $PbTiO_3$ sol-gel solution. The solution was then allowed to cool. During this process 2 mL of EtOH was added to the solution. A second solution composed of 4.548 g of $Ti(OPr^i)_4$ or 4.251 mL of $Ti(OBu)_4$ and 5 mL of EtOH or 5 mL of MeOEtOH was made. The titanium solution was added to the room temperature lead solution resulting a clear and colorless solution. Membranes were dipped into this solution for one minute and then allowed to air dry for 30 minutes. Three sets of membranes were then calcined in the air at a ramp rate of 50 °C/hr to temperatures of 550 °C and 650 °C and held for six hours followed by cooling to room temperature at 30 °C/hr. The remaining solution was used to make bulk powder samples of $PbTiO_3$ for comparison of *d*-spacing from the electron diffraction pattern of the nanotubes to d spacing determined from the powder X-ray diffraction. The other compounds were prepared by the above way.

Characterization Methods. Scanning electron microscope (SEM) images were obtained using the following procedure. The calcined membrane was adhered to a

piece of paper towel using epoxy. After the membrane was set, the surface film was removed by polishing. The alumina template was removed by immersing the sample in 6 M NaOH for 1 hour. After soaking in base, the sample was washed in distilled water to remove the NaOH. After drying overnight in air, the samples were attached to SEM stubs using double-sided Cu tape. Using an Anatech sputter coater, 20 nm of Au was applied to surface. Images were taken on a Phillips 505 microscope. Energy dispersive X-ray spectroscopy (EDS) analysis was performed in the SEM using a Kevex Super 8000 Microanalyzer.

Transmission electron microscope (TEM) images were obtained by grinding up the calcined membrane with a mortar and pestle. The powder was then allowed to soak in NaOH solution for 1 hour. The solution was then decanted off and the remaining powder was rinsed several times with purified water. A layer of water was left so that a pipette could be used to transfer both water and powder onto a formvar coated 200 mesh copper grid. Excess water was removed with a syringe and the sample was allowed to dry overnight. Images and electron diffraction patterns were taken on a JEOL 2000 microscope. The accelerating voltage was 100 kV and the camera length was 120 cm.

Powder X-ray diffraction data were collected on a Phillips PW1830 diffractometer with Cu K_α radiation (1.5406 Å).

Raman spectra were obtained using a Nicolet Magna-IR spectrometer with FT-Raman module attachment using a Nd:YAG excitation laser (1064 nm).

Permittivity (ε') measurements were taken on a TA Instruments DEA 2970 Dielectric Analyzer using parallel plate capacitor sensors. Samples underwent a temperature ramp frequency sweep program mode. The temperature range measured was from 30 °C to 400 °C and frequency range was 1-10,000 Hz.

Curie temperature and melting point measurements were taken on a TA Instruments Thermal Analysis & Rheology DSC 2010 and high temperature (1600 °C) DTA by using aluminum pans and aluminum oxide crucibles as holders, respectively. Samples underwent a temperature ramp sweep program mode. The standard materials were just aluminum pans for DSC and α-Al_2O_3 for DTA. The temperature range measured was from 50 °C to 600 °C for DSC analysis and from 50 °C to 1600 °C for DTA analysis, respectively.

RESULTS AND DISCUSSION

Synthesis of ABO_3 Nanotubes on AlO_x membrane

The synthesis of the perovskite nanotubes made by sol-gel template synthesis.[5] The perovskite ABO_3 nanotubes were prepared with a chelate sol-gel of titanium isopropoxide ($Ti(OPr^i)_4$) and the respective metal acetate. Whatman® anodisc membranes, with a 200 nm pore size, served as the template.

Membranes dipped into the ABO_3 sol-gel for one minute led to the formation of nanotubes. Masking off one side of the membrane was helpful in preventing surface film formation that hindered the identification the nanotubes. The template was allowed to air dry and then calcined at 650 °C.

PZT Solid Solutions

A solid solution is a crystalline phase that has variable composition. The compound $PbZrO_3$ exhibits a continuous substitutional solid solution with $PbTiO_3$. Unit-cell volumes in the series $PbZr_{1-x}Ti_xO_3$ continuously decrease as the composition of Ti, x increases for x= 1. Because of the structural similarities among the materials, $PbTiO_3$ and $PbZrO_3$, the data are consistent with complete solid solubility across the entire range of x with Vegards law (*Fig.* 2).

Morphological Characterization of ABO_3 Tubes

Initial SEM images looked like the known thin films are of a calcined sample prior to polishing. We already identified what film formation looks like on top of the AlO_x template made from the 0.8 M sol-gel solution at the previous experiment. Previous attempts in using 0.1 M, 0.5 M and 0.6 M solutions resulted in no surface film formation and were therefore abandoned. *Fig.* 3 shows an SEM image of $PbTiO_3$ structures obtained after removal of the template. The sample $PbTiO_3$ shown was calcined at 650 °C. Higher magnifications of the structures show surface film still present on top of structures, which prevented the distinction between tube or fiber formation.

Microanalysis of the structures and remaining surface film by EDS confirmed the presence of (Pb, Ti) of $PbTiO_3$, (Pb, Zr; *Fig.* 4b)) of $PbZrO_3$ and (Pb, Zr, Ti) of $PbZr_{1-x}Ti_xO_3$ on both surface film and structure areas for each

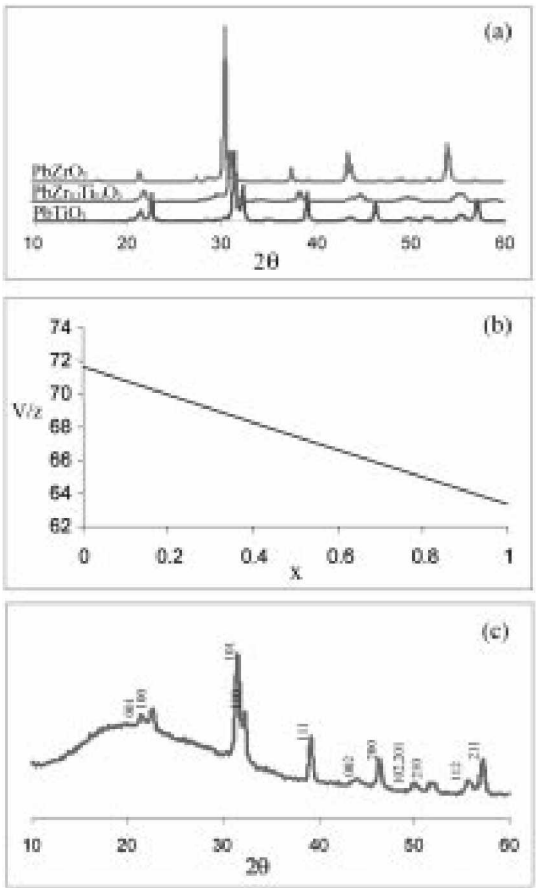

Fig. 2. (a) Powder X-ray diffraction trace of the $PbZr_{1-x}Ti_xO_3$ system. (b) Graph of the continuous substitutional solid solutions of the series $PbZr_{1-x}Ti_xO_3$; V is Volume, z is the number of fomula in the unit cell, and x is the composition of Ti. (c) Nanotubes X-ray diffraction trace of $PbTiO_3$ with AlO_x membrane.

perovskite. However, this experiment did confirm the absence of template material on surface of structures.

To evaluate whether tube or fiber formation occurred, the template was masked off on one side prior to being dipped into the sol-gel solution. The same procedure as described above was followed and the sample was fired at 650 °C.

Fig. 4 shows cross-sectional SEM pictures of PZT structures obtained after removal of template. It should be noted that the thickness, with adequate sand on the surface of films and without AlO_x membrane in the 6 M-NaOH, was about 50 mm lengths.

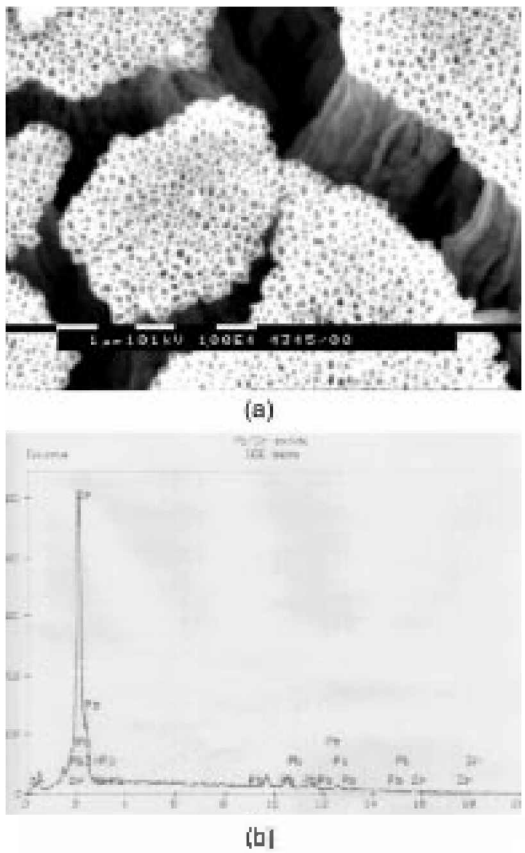

Fig. 3. (a) Top view of $PbTiO_3$ bundle illustrating formation of open tubes with an outer diameter of 200 nm. (b) Energy dispersive X-ray spectrometry analysis with the presence of (Pb, Zr) on $PbZrO_3$ bundle.

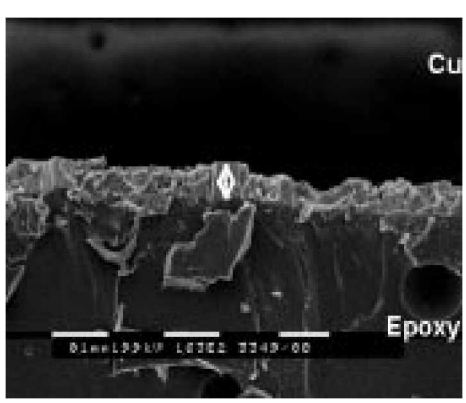

Fig. 4. SEM images of 50 μm(↕)-thickness $PbZr_{1-x}Ti_xO_3$(x=0.6) film: Cross-sectional SEM picture of PZT film on epoxy.

Structural Characterization of ABO_3 Tubes Powder and Nanotubes X-ray Diffraction. The bulk

material heated to 650 °C and 900 °C was analyzed using powder x-ray diffraction (XRD). As shown in *Fig.* 2, each powder pattern had peak positions in good agreement with the tetragonal phase indexed by the software library. The results of the powder pattern indexing made standard identification because thin films made with similar sol-gel synthesis methods were reported to have ferroelectric behavior when crystallized at 650 °C. However, the nanotube patterns itself indicated that the cubic phase and the tetragonal phase were present depending on particle sizes. If the tetragonal phase were present in the bulk powder, the lower symmetry of the unit cell would cause more diffraction lines to appear.[6] The increase in the number of lines is due to the introduction of new plane spacing, caused by a non-uniform distortion.[6] The tetragonal phase of $PbTiO_3$ and $BaTiO_3$ is often identified by the characteristic peak separation of the (200) and (002) diffraction lines near 2θ=43 and 46°, respectively.[7-10] *Fig.* 5 also shows that there are two displacive phases, cubic and tetragonal phases of nanotubes depending on $PbTiO_3$ crystallite sizes. We will describe in more detail about that at the section of crystallite sizes and Raman spectroscopy.

Crystallite Sizes. The study of nanomaterials has become an important aspect in learning how size influences properties of the material in question and it has been observed that size does matter. An example of how nanoscaling materials can influence properties can be seen through the work of Lubrosky who has shown that ferromagnetic particles isolated by a nonmagnetic matrix, has an increase in coercive force as the particle size is reduced from micrometers to the nanometer scale.[11,12]

This observation is related to the magnetic domains present in the material. At the micrometer size each particle contains several magnetic domains that contribute to the coercive force, but as the particle size decreases, each particle now becomes a single-domain. The size was determined by X-ray analysis with the aid of Scherrer's equation, transmission electron microscopy (TEM) and Raman spectroscopy[13,14] (*Fig.* 5 and *Table* 1). We identified that an apparent tetragonal phase was shown above 15.4 nm of particles size. Instead the particles size dependence of the polycrystalline phase was observed by XRD patterns in the nanobundles. The critical particles size, size effects on phase changing from tetragonal to cubic, will be currently being considered.

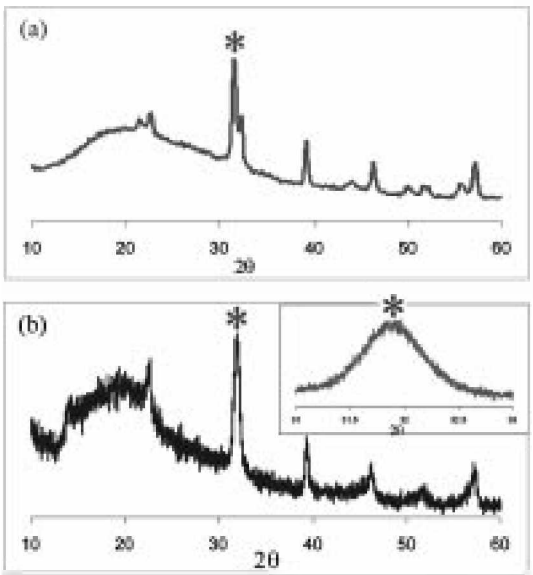

Fig. 5. Nanotubes X-ray diffraction trace of two displacive phases: (a) Tetragonal phase of $PbTiO_3$. The crystallite size (*) is 29 nm. (b) Polycrystalline phase of $PbTiO_3$. The crystallite size (*) is 11.2 nm.

Raman Spectroscopy. Bulk samples were analyzed with Raman spectroscopy to confirm the symmetry in the unit cell. *Fig.* 6 shows spectra for powders calcined at 650 °C and 900 °C and *Table* 2 and 3 summarizes peak

Table 1. Tetragonality (c a) and crystallite sizes of the $PbTiO_3$ powder and nanotubes (calcination temperature: 650 °C)

Sample type	Tetragonality c (Å)/a(Å)	Grain size	Calculation method
Nanotubes	≈1 4.1262 3.9311 =1.0496 4.1176 3.9027 =1.0551	~15 nm 25 nm 29 nm	-Scherrer's equation -TEM -Raman spectra -Scherrer's equation

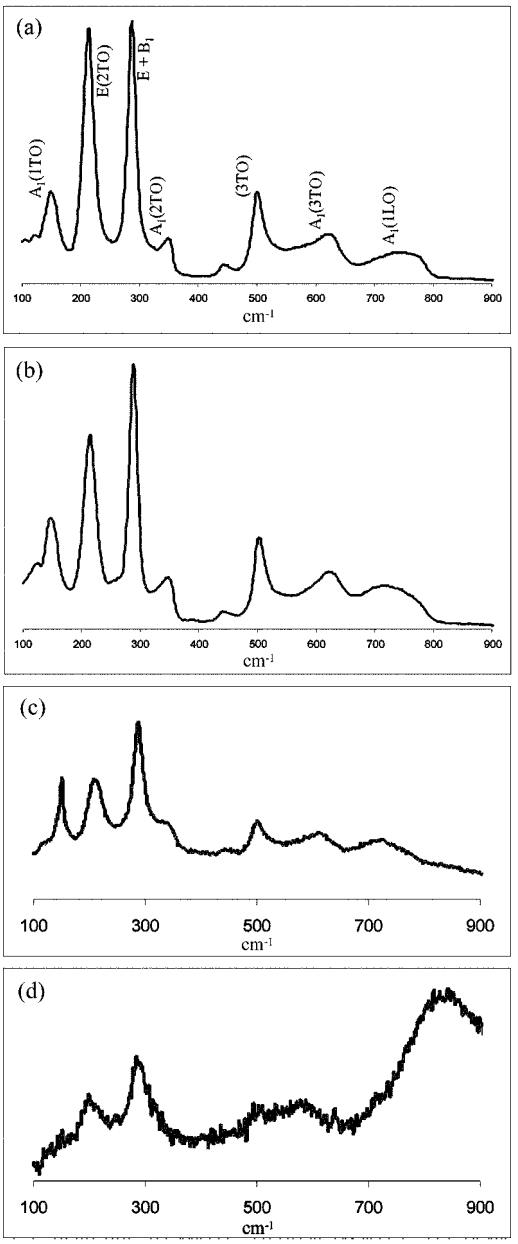

Fig. 6. Raman spectra identified by changing of the relative intensities of E+B1 and E(2TO) soft modes according to particle sizes: (a) Bulk $PbTiO_3$ powder calcined at 900 ℃. (b) $PbTiO_3$ powder calcined at 650 ℃. (c) Tetragonal phase of $PbTiO_3$ nanotubes calcined at 650 ℃. (d) Polycrystalline phase of $PbTiO_3$ nanotubes calcined at 650 ℃.

positions observed for each spectrum. Based on group theory all four of the optical modes of cubic perovskite-type materials should be Raman inactive whereas seven of the optical modes for the polar tetragonal phase should be Raman active.[7,15] Peaks observed in $PbTiO_3$ nanotubes spectrum shown in *Fig.* 6 imply that the local symmetry of the sol-gel processed $PbTiO_3$ is not the lower symmetry of the tetragonal phase determined by XRD and therefore the nanotubes are not phase pure at a critical particles size.

Table 2. Peak positions in Raman spectra of the $PbZr_{1-x}Ti_xO_3$ systems (Rxn. Temp.: 650 ℃)

Unit: cm^{-1}

Composition of Ti	Soft Mode	
x	A_1(1TO)	E(2TO)
1	149.14	211.45
0.9	145.71	203.88
0.8	145.18	197.63
0.6	142.11	196.07

Submicron phase pure tetragonal $PbTiO_3$ powders made through hydrothermal synthesis showed Raman spectra (*Table* 2) where eight peaks at 86, 106, 142, 213, 287, 337, 504 and 613 cm^{-1} confirmed the phase.[7,13,14] Nanotubes that are not phase pure can show Raman activity. Powders prepared using a sol-gel method at a low temperature of 400 ℃ also showed Raman activity in powders that were determined to be phase transition between C_{1v} and C_{3v} point groups induced by the size reduction.[16] The authors explain that the Raman spectra indicated the existence of a stable ferroelectric phase in the $PbTiO_3$ nanocrystals at room temperature. They showed that the 7 nm particles of the $PbTiO_3$ exhibited unique spectral features that were different from those of crystals to the amorphous powder and 17 nm particles nanoscale. The Raman spectrum of a 17 nm average size was also observed in our spectra as the calcinations temperature increased.

Zhou, Zhang, Chen and Choy's study on grain size effects on structure made by sol-gel processing also report similar values for powders that were determined to be particles size by XRD and the effects of the particles size by the Raman.[17,18] They discuss that the Raman activity of the particles size determined by XRD is attributable to the vibrational modes at room temperature of ultrafine $PbTiO_3$ particles. They also refer that the Raman peaks exhibit downshift in frequency, broadening and intensity changes with decreasing particle size. *Fig.* 6 shows that

Table 3. Phonon energies in $PbTiO_3$ powder calcined at 650 ℃ and relative intensities of Raman peaks in $PbZr_{1-x}Ti_xO_3$ powder

(a) Phonon energies in $PbTiO_3$ powder (calcinations temperature: 650℃)

Mode	A_1(1TO)	E(2TO)	$E+B_1$	A_1(2TO)	E(3TO)	A_1(3TO)	A_1(1LO)
Energy(cm^{-1})	147.17	214.51	288.25	347.40	503.49	623.13	715.57

(b) Relative intensities of Raman peaks in $PbZr_{1-x}Ti_xO_3$ powder (tetragonal phase)

Composition of Ti X	1.00	0.90	0.80	0.60	0.52
rel. $I_{E(2TO)}$/rel. I_{E+B1}	0.729	0.876	0.953	1.016	0.965

the Raman activity of the apparent cubic phase determined by a XRD pattern (*Fig.* 5). The vibration peak of A_1 (1TO) mode disappears when the particle size is 11.2 nm as determined by XRD. Generally, the Raman peaks broaden with decreasing a particle size. The Raman spectra show that the small particles size nanotubes were not phase pure. This may have caused the peak positions to match up with the cubic phase. Through the method of comparative *d*-spacing, the nanotubes must be assigned the cubic phase, as grain size was reduced. Instead the grain size dependence of the paraelectric phase was observed.

Transmission Electron Microscopy and Electron Diffraction. Imaging by TEM revealed that the tubes observed in the SEM images are comprised of small grains (*Fig.* 7). The electron diffraction region selected was the center of the structures imaged at 40,000X magnification. The diffraction pattern indicated that the grains of the tubes are polycrystalline (*Fig.* 7). The powder rings resulting from the electron diffraction were indexed to the XRD of the bulk material by the method of comparative *d* - spacing.

D-spacing can be calculated from the diameters of the diffraction rings using the following equation $dr=l\lambda$, where d is the calculated *d*-spacing in Ångstoms, r is the radius of the diffraction rings in mm, *l* is the camera length in mm, and e is the wave length of the electrons in Å.[1] To reduce error, a ratio of each ring radius to the centermost ring is calculated and compared to the ratio of corresponding *d*-spacing of the bulk $PbTiO_3$ powder.

$$r\,(\text{outer})/r\,(\text{inner}) = d\,(\text{inner})/d\,(\text{outer})$$

Table 4 summarizes measured and calculated values. The ratio calculated from the diffraction pattern is close in value to the powder pattern for the cubic phase. Also, we identified that the nanotubes were capped in the bottom coating side of the template and the grain size of

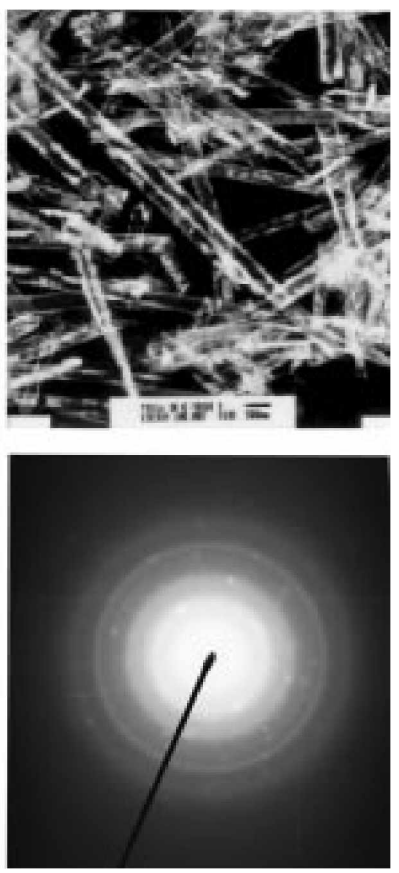

Fig. 7. (a) TEM images and (b) Electron diffraction pattern of the $PbTiO_3$ nanotubes: TEM images and electron diffraction pattern for both perovskites that the structures observed in *Fig.* 5 comprose small grains that are polycrystalline with single in some of samples.

$PbTiO_3$ was about 12 nm through TEM images.

Dielectric Analysis of Structures. A temperature ramp/frequency sweep program was chosen to determine the appropriate frequency to measure dielectric permittivity (ε') and also to evaluate the nanostructures phase. Dur-

Table 4. Measured radius values from the electron diffraction of $PbTiO_3$ nanotubes and d-spacing from the powder pattern are shown: ratios are close in value

d-spacing(A)	Radius(mm)	Ratio of radii	Ratio of d-spacing
d_1=3.9209	r_1=3.3	r_2/r_1=1.33	d_2/d_1=1.40
d_2=2.8008	r_2=4.4	r_3/r_1=1.52	d_3/d_1=1.71
d_3=2.2929	r_3=5.0	r_4/r_1=1.89	d_4/d_1=2.00
d_4=1.9577	r_4=6.2		

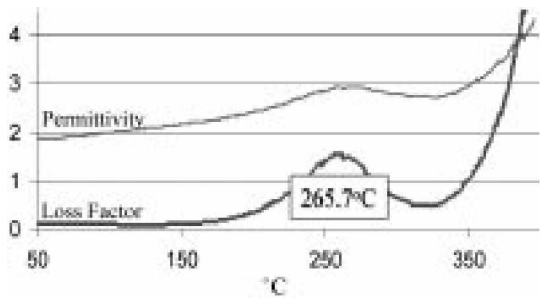

Fig. 8. Graph of loss factor vs. temperature 1 Hz for the $PbTiO_3$ nanotubes with AlO_x membrane(thickness of nanotubes: 0.0607 mm; method: temperature ramp).

ing the analysis, it was determined that 1 Hz was the appropriate frequency to measure permittivity. The dielectric properties of $PbTiO_3$ is temperature and phase dependent.[1,2,4,19,20] The phase transition from ferroelectric to paraelectric behavior occurs at 490 °C and at this temperature, a maximum ε' can be measured. But we measure the dielectric constants of $PbTiO_3$ between 30 °C and 450 °C according to the instrument specification.

Fig. 8 shows the dielectric constants of $PbTiO_3$ with temperature dependence of the alumina template: The sample size is 0.0607mm thickness with AlO_x template. At 265.7 °C ε' is 2.87 with a maximum peak. This is the other evidence of Curie temperature in the PT nanotubes.

Curie Temperatures and Melting Point of Nanotubes. DSC and DTA experiments were performed on a computer controlled DSC 2010 and high temperature (1600 °C) DTA of TA instruments thermal analyzer. Typically, a sample (~2 mg) of nanotube crystalline material was obtained from $PbTiO_3$ coating on the AlO_x membrane and then removing the AlO_x membrane in the 6M-NaOH solution. The samples were heated to 600 °C for DSC analysis and 1600 °C for DTA analysis at 10 °C/min, respectively. A size effect on the ferroelectric phase transition in $PbTiO_3$ and PZT particles and nanotubes was

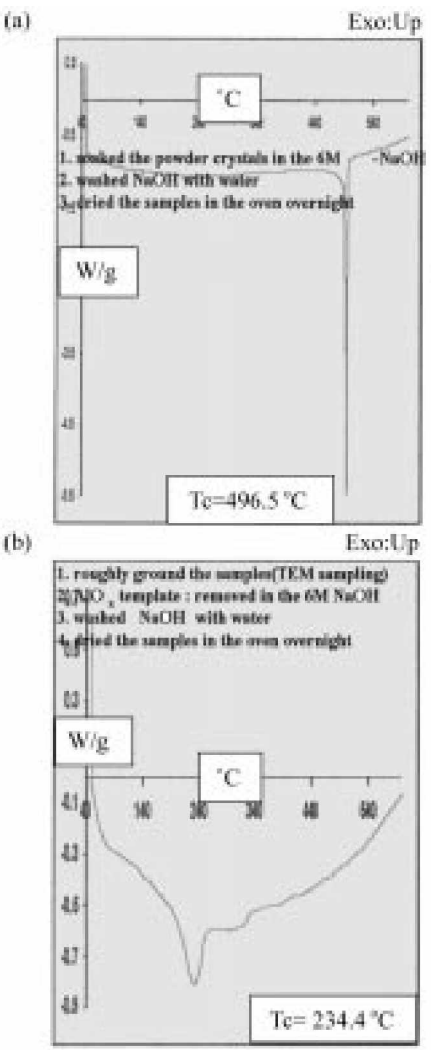

Fig. 9. Curie temperatures of $PbTiO_3$ powder and nanotubes: (a) Bulk powder calcined at 900 °C with treatment of 6M-NaOH. (b) Nanotubes calcined at 650 °C without AlO_x membrane in the 6M-NaOH.

investigated by using DSC analyses (*Fig.* 9 and *Table* 5). Ishikawa *et al.*[12] investigated the effect of particle size on

Table 5. Curie temperatures of $PbZr_{1-x}Ti_xO_3$ powder and nanotubes

Composition of Ti x	Curie temperature	Calcination temperature	Material type
1	496.5 °C	900 °C	Powder
	489.7 °C	650 °C	Powder
	234.4 °C	650 °C	Nanotubes
	248.0 °C		
0.9	476.1 °C	900 °C	Powder
	476.9 °C	650°C	Powder
	236.9 °C	650 °C	Nanotubes
	266.0 °C		
0.8	451.9 °C	900 °C	Powder
0	229.7°C	900 °C	Powder
	213.7 °C	650 °C	Powder
	123.6 °C		Nanotubes

the ferroelectric phase transition temperature in the $PbTiO_3$ powder materials. The DSC analysis of bulk $PbTiO_3$ powder fired at 900 °C showed the Curie temperature was 496.5 °C, while the DSC analyses of bulk $PbTiO_3$ nanotubes indicated that Curie temperatures were large temperature ranges, from 234.4 °C to 282.7 °C, depending on the particle sizes and on the aging of a solution processing. The above-phenomenological discussion on the ferroelectric phase transition show that the anomalous Curie temperature shifts toward lower temperature, as the particles size of powder and nanotubes becomes small. The melting point of $PbTiO_3$ nanotubes was measured by using DTA analysis (*Fig.* 10). The melting point of $PbTiO_3$ nanotubes showed a large depression, 1207°C with decreasing size, as a larger fraction of the total number of atoms is on the surface. As a standard material, the melting point of $PbTiO_3$ powders calcined at 900 °C was 1271 °C. Thermodynamic models based on differences in surface tension between the liquid and solid can be applied to this system, even though the bonding is highly directional.[21]

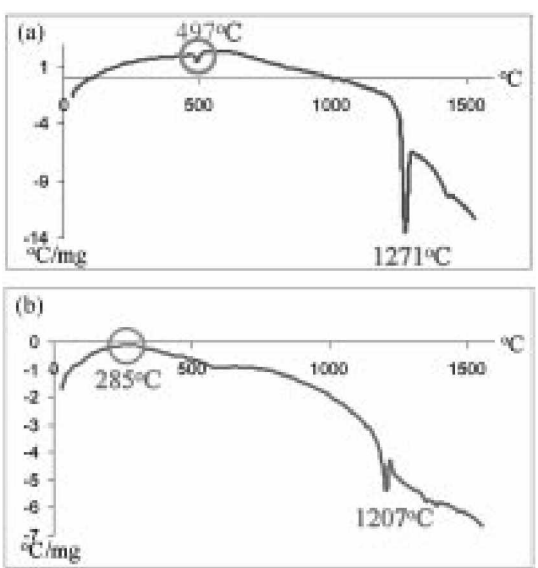

Fig. 10. Melting points of $PbTiO_3$ (a) powder and (b) nanotubes without AlO_x membrane in the 6M-NaOH are measured by DTA.

Acknowledgments. This work was in progress with the aid of PKD at chemistry department of Colorado State University for the period of my sabbatical, from February 15, 2001 to February 22, 2002. KSC would like to thank Prof. Peter K. Dorhout (PKD), Prof. Ellen R. Fisher and Ph.D. student, Bernadette A. Hernandez also at the chemistry.

REFERENCES

1. Mitsui, T.; Tatsuzakai, I.; Nakamura, E., Eds. *An Introduction to the Physics of Ferroelectrics; Gordon and Breach Science Publishers*: New York, 1976.
2. Akdogan, E. K.; Leonard, M. R.; Safari, A. *Size Effects in Ferroelectric ceramics*; Nawala, H. S., Eds.; Handbook of Low and High Dielectric Constant Materials, Vol.; Academic Press: San Diego, 1999; 61.

3. Jona, F.; Shirane, G. *Ferroelectric Crystals*; MacMillan: New York, 1962.
4. Sharma, H. B.; Mansingh, *A. J. Mater. Sci.* **1998**, *33*, 4455.
5. Hernandez, B. A.; Chang, K. S; Fisher, E. R; Dorhout, P. K. *Chem. Mater.* **2002**, *14*, 480.
6. Cullity, B. D. *Elements of X-Ray Diffraction; Addison-Wesly: Massachusetts*. 1978.
7. Asiaie, R.; Zhu, W.; Akbar, S. A.; Dutta, P. K. *Chem. Mater.* **1996**, *8*, 226.
8. Golego, N.; Studenikin, S. A.; Cocivera, M. *Chem. Mater.* **1998**, *10*, 2000.
9. Yukawa, K.; Wakino, K. *Interg. Ferroelect.* **1998**, *20*, 107.
10. Ma, Y.; Vileno, E.; Suib, S.; Dutta, P. K. *Chem. Mater.* **1997**, *9*, 3023.
11. Lubrosky, F. E. *J. Appl. Phys.* **1961**, *32*, 171S.
12. Weissmuller, J. In *Nanomaterials: Synthesis, Properties and Applications*; Cammarata, A. S. E. a. R. C., Ed.; Institute of Physics Publishing: London, 1996; p 266.
13. Ishikawa, K.; Yoshikawa, K.; Okada, K. *Phys. Rev. B*, **1988**, *37*(10), 5852.
14. Zhang, W. L.; Jiang, B.; Zhang, P. L.; Ma, J. M.; Cheng, H. M.; Yang, Z. H.; Li, Z. H. *J. Phys.: Condens. Matter*, **1993**, *5*, 2619.
15. Fately, W. G.; Dollish, F. R.; McDevitt, N. T.; Bently, F. F. *Infared and Raman Selection Rules For Molecular and Lattice Vibrations; Wiley-Interscience: New York*, 1972.
16. Fu, D.; Suzuk, H.; Ishikawa, K. *Phys. Rev. B*, **2000**, *62*(5), 3125.
17. Blum, J. B. *Mat. Lett.*, **1985**, *3*(9-10), 360.
18. Zhow, Q. F.; Zhang, J. X; Chan, H. L. W.; Choy, C. L. *Ferroelectrics*, **1997**, *195*, 211.
19. Frey, M. H.; Han, Z. X. P.; Payne, D. A. *Ferroelectrics* **1998**, *206*, *207*, 337.
20. Kamalasanan, M. N.; Kumar, N. D.; Chandra, S. J. *Appl. Phys.* **1993**, *74*, 5679.
21. Goldstein A. N.; Echer, C. M.; Alivisatos, A. P. *Science* **1992**, *256*, 1425.